Available online at www.sciencedirect.com
SCIENCE DIRECT®
Catalysis Today 97 (2004) 55–61
CATALYSIS TODAY
www.elsevier.com/locate/cattod

Structural characterization of porous film materials and the supported metal catalysts by synchrotron powder X-ray diffraction

Hwo-Shuenn Sheu [a,*], Pang-Hung Liu [b], Hsin-Ling Cheng [b,1], Kuei-jung Chao [b], Yen-Po Chang [b]

[a] *National Synchrotron Radiation Research Center, Hsinchu, Taiwan*
[b] *Department of Chemistry, National Tsinghua University, Hsinchu, Taiwan*

Received 7 January 2004; received in revised form 1 April 2004; accepted 8 May 2004
Available online 20 July 2004

Abstract

Synchrotron powder X-ray diffraction (PXRD) was applied to the structural characterization of microporous and mesoporous materials as well as their supported metal catalysts. Advantages of synchrotron X-ray powder diffraction are illustrated by the detection of the MFI crystalline phase on the non-smooth surface of a microporous MFI film supported on the inner wall of a ceramic hollow tube, and of the formation of Au and Pt nano-particles in powdery mesoporous materials.

Keywords: Porous materials; Nano metal particles; Synchrotron PXRD

1. Introduction

X-rays from a synchrotron radiation source exhibit high brilliance, high collimation, tunable wavelength over a wide range of energy, polarization (linear, elliptical and circular) and short pulse length (tens of ps) over a wide range of pulse period (2–400 ns) [1]. It thus makes possible the study of a trace amount of a crystalline sample, and the nanosized crystals that usually possess very weak scattering power. The high intensity of the X-ray beam shortens sample exposure time and is suitable for in-situ study of crystal growth under non-ambient conditions [2–4], while the highly collimated synchrotron beam can reduce the error caused by samples with a non-smooth surface. The combination of synchrotron X-rays with a large diffractometer can simultaneously provide high energy resolution and high spatial resolution powder diffraction [5]. The Rietveld refinement analysis of PXRD data is powerful for studying the crystal structure of catalysts and nano size metals in general [6]. In this study, the advantages of synchrotron powder X-ray diffraction (PXRD) with Rietveld refinement analysis are demonstrated in the detection of MFI zeolite in a tubular filter, and nanostructured metals in mesoporous materials.

2. Experimental

2.1. Preparation of samples

An MFI (pore opening of 5–6 Å) membrane was fabricated on a commercial alumina tube (denoted as GU, Inoceramic Inc., Germany) made of a γ-Al_2O_3 layer of 5 nm pore opening at the innermost position and a macroporous α-Al_2O_3 layers of average pore sizes decreasing from the external to the internal layer. To prepare a zeolite MFI membrane, a GU tube was first immersed in a clear solution of TPAOH-TEOS-H_2O mixture under hydrothermal conditions at 100 °C for 15 h. The molar composition of the solution was 9TPAOH:25TEOS:480H_2O. After being calcined at 500 °C, the tube was treated by secondary in-situ synthesis at 100 °C for 12 h in a diluted reaction sol and subsequently by the vapor phase transport method at 100 °C using TPAOH and H_2O as the vapor phase. Finally, the coated zeolite was calcined at 400 °C.

* Corresponding author. Tel.: +886-35780281/7122; fax: +886-35783813.
E-mail address: hsheu@nsrrc.org.tw (H.-S. Sheu).
[1] Present address: Department of Chemistry, National Taiwan University, Taipei, Taiwan.

0920-5861/$ – see front matter © 2004 Elsevier B.V. All rights reserved.
doi:10.1016/j.cattod.2004.05.017

A mesoporous silica membrane was supported on an alumina tube of multilayer α-Al_2O_3 (denoted as CU, US filter) with an α-Al_2O_3 layer of 200 nm pore opening at the innermost position. A silica precursor prepared by a sol gel process was dip-coated on the inner side of a CU tube, while the outer side of the tube was tightly sealed by a sumitube. The molar composition of the precursor was 0.1CTAB:1TEOS:3.5H_2O:0.005HCl:20EtOH. After baking at 105 °C and calcination at 550 °C, a mesoporous silica membrane was obtained. The α-Al_2O_3 supported mesoporous silica membrane was then treated by following the synthesis process above for an MFI membrane, to give an MFI/meso-silica composite membrane.

A novel template synthesis of densely packed or highly dispersed metal nanostructures in functionalized mesoporous silicas was developed by us recently [7]. Following the method of our previous work, nanostructured Au and Pt were prepared in one dimensional mesoporous silica SBA-15 and three dimensional mesoporous MCM-48, respectively. Siliceous SBA-15 was synthesized using $(EO)_{20}(PO)_{70}(EO)_{20}$ triblock copolymer (P123) as template [8]. The template-free SBA-15 was modified with N-trimethoxysilylpropyl-N,N,N-trimethylammonium chloride (TPTAC, 50 wt.% in methanol, Gelest) [9] to give SBA-15-PTA^+Cl^-. The dried SBA-15- PTA^+Cl^- was suspended in a $HAuCl_4$ aqueous solution at pH = 2 and 8, which was adjusted by adding the NaOH aqueous solution. The resulting solid samples were filtered, dried and then reduced in hydrogen gas at 300 °C to give Au(2) and Au(8)-1. Another portion of the sample prepared under pH = 8 was washed very carefully with de-ionization water before reduction and to give Au(8)-2.

MCM-48 was synthesized using CTAB (cetyltrimethylammounium bromide) and Brij-30 ($C_{12}H_{25}O(C_2H_4O)H_4$, $C_{12}EO_4$) as templates [10], calcined and then modified with TPTAC to give MCM-48-PTA^+Cl^-. This was mixed with an aqueous solution of H_2PtCl_6. After filtration and drying at ambient temperature, the platinum was reduced in H_2 flow under heating from room temperature to 300 °C with a 5 °C/min heating rate, resulting in Pt nanostructures in MCM-48.

2.2. Characterizations

MFI zeolite of the calcined membranes was examined by X-ray diffraction performed on a MAC Science, M18X® rotating anode powder diffractometer using Cu Kα1 (λ = 1.5406 Å) radiation operated at 50 kV and 200 mA as well as by synchrotron PXRD carried out on beamline BL17A of the National Synchrotron Radiation Research Center (NSRRC), Taiwan, using the grazing incidence technique (Fig. 1a).

The structure of the metals was characterized by PXRD conducted on beamline BL17A in NSRRC, Taiwan. The X-ray wavelength was 1.32633 Å, and the diffraction signals were accumulated for ∼15 min and recorded by an

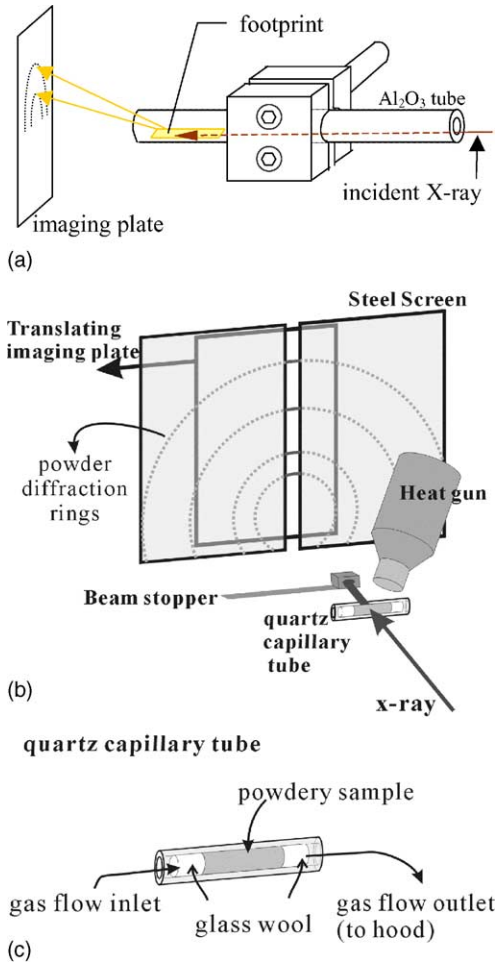

Fig. 1. Scheme of the synchrotron PXRD setup for MFI film supported on a ceramic tube (a) and for in-situ study of Pt metal growth in mesoporous SiO_2 powder (b) and (c).

imaging plate positioned 0.12 m away from the sample. The crystal growth of Pt metal in three dimensional mesoporous MCM-48 was monitored by an in-situ PXRD. The sample was packed into a capillary tube and heated to 300 °C with a 5 °C/min heating rate under H_2 flow and held at 300 °C for a certain time period, using the synchrotron radiation light source and an imaging plate as the detector (Fig. 1b).

TEM with EDS was carried out on a JEOL JEM-2010 electron microscope equipped with an Oxford EDX analysis system. Samples were embedded in resin and solidified at 60 °C for 12 h, then ultramicrotomed into slices with a thickness of ∼50 nm.

2.3. Rietveld method

The Rietveld refinement method is applied on diffraction data which contain majority known structural information with minor modifications of structures or chemical compositions. The method was first developed to refine crystal structure based on full diffraction profile analysis by Rietveld in 1969 [6]. The powder X-ray diffraction pattern was

recorded by step scan with a typical step width of 0.02° in 2θ.

Y_i represent the diffraction intensity at step i that may contain contributions from several Bragg reflections, such as

$$Y_i = s \sum_k M_k L_k |F_k|^2 P(\theta_i - \theta_B) O_k + Y_{ibck}$$

where s is a scale factor; Σ_k means the sum over all k Bragg reflections; M is the multiplicity factor; L is the Lorentz and polarization factor; F is the structure factor, P is the profile function; θ_i is the diffraction angle of the i step; θ_B is the Bragg angle of reflection k; O is the preferred orientation function; Y_{ibck} is the background at step i. During the refinement, the quantity minimized is the weighted sum of the squares of the differences between observed and calculated intensity at each step. This is

$$\text{wRp} = \sum_i w_i |Y_{iobs} - Y_{ical}| / \sum_i (Y_{iobs})$$

In this study, the metal diffraction data of highly dispersed Pt and Au nanostructures were analyzed and refined by the Rietveld method using the GSAS program [11]. The calculated diffraction profiles were based on Pseudo–Voigt (Gaussian plus Lorentzian) distribution and broad peak widths.

3. Results and discussion

3.1. MFI zeolite film

Zeolites are microporous crystalline materials, used routinely as shape selective catalysts. They are also known as 'molecular sieves', due to their pore size on the molecular level, because such minute pores can block large molecules and allow the passage of only smaller ones [12,13]. If a zeolite can be grown into a thin and continuous membrane on a porous support, it should work just as a conventional sieve but with mesh size on the molecular level. With a thin zeolite membrane, separation may then be achieved under a steady state condition where adsorption occurs on one side and continuous desorption occurs on the other side. If catalytic reaction processes are operated under a steady state, the integration of a zeolite membrane into a catalytic reactor will be quite attractive [14,15]. To maximize the throughput, the zeolite layer must be very thin, and the detection of zeolite on substrate samples thus becomes difficult.

After calcination, an MFI film of about 1.5 μm thickness on a GU tube was observed by scanning electron microscopy (SEM) (Fig. 2). Detection of a crystalline MFI zeolite layer is very difficult with a conventional powder X-ray diffractometer, even with the inner surface of the cut pieces from an MFI/Al_2O_3 tube facing the incident X-ray beam (a

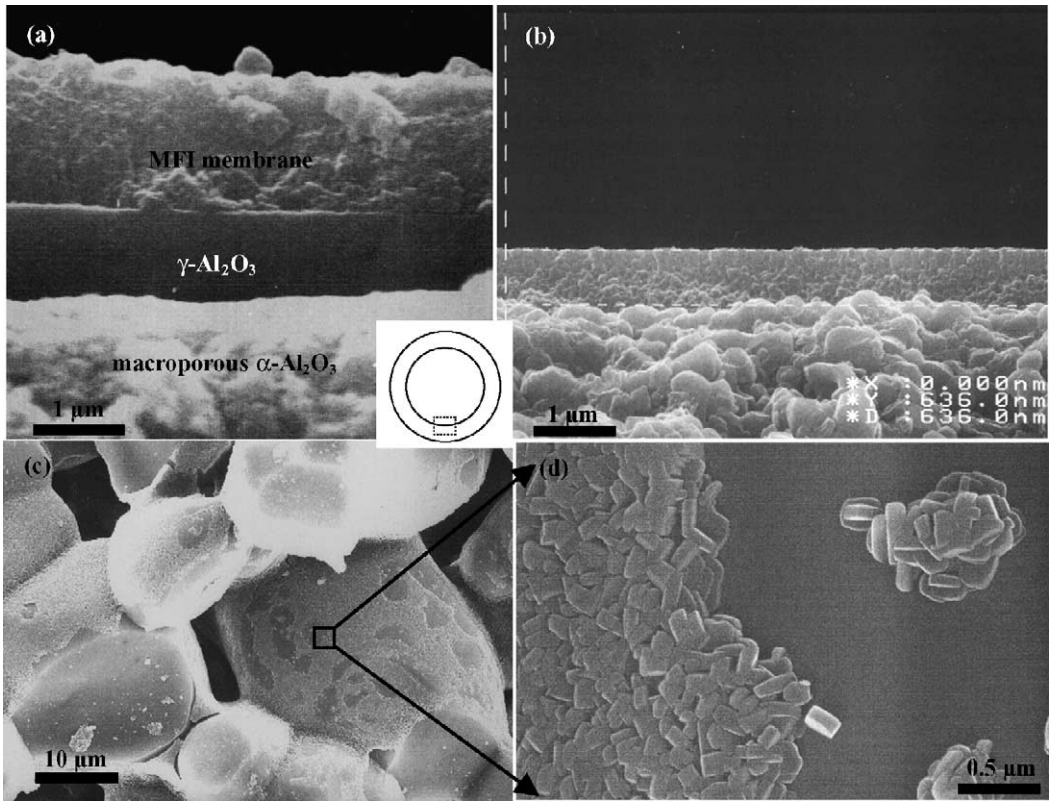

Fig. 2. SEM of MFI zeolite films on a GU-Al_2O_3 tube (a), and on a mesoporous-silica/CU-Al_2O_3 tube (b), SEM of a macroporous Al_2O_3 layer of MFI/mesoporous-silica/CU tube (c) and (d).

destructive method). Because of the very thin nature of the MFI zeolite layer and the curved shape of the specimen, the membrane generates very weak scattering signals of MFI and a strong PXRD pattern of the Al_2O_3 support as shown in Fig. 3a. However, by using synchrotron X-rays, it is possible to obtain the powder diffraction signal of MFI with almost complete absence of the PXRD pattern of the Al_2O_3 support on a ceramic-tube supported sample (Fig. 3b). Fig. 1a shows the setup for measuring synchrotron X-ray powder diffraction of a MFI/Al_2O_3 composite tube with about 10 mm diameter hole opening. The ceramic tube was fixed at the center of a Huber 5020 diffractometer with its hole axis along the X-ray beam direction. In order to reduce the signal derived from the Al_2O_3 substrate, the incident beam hits a ceramic tube with a grazing angle to the inner wall and about 10 mm from the end of the outgoing opening. During the X-ray diffraction measurement, the tube was held still and the imaging plate collected two theta angles up to 45°, and this is considered quite adequate to characterize an MFI sample. The PXRD pattern of MFI on the inner wall of the tube is similar to that in its powder form as shown in Fig. 3b. The relative intensity of the PXRD signal at the low angle of the tubular sample is much higher than that of the high angle signal, and is due to the blockage of some of the X-ray beams by the tube. The limitation is thus set by the distance of the tube opening from the center of the incident beam at the tube. This result indicates that synchrotron powder X-ray diffraction is suitable to measure samples with a non-smooth surface even on a hollow tube.

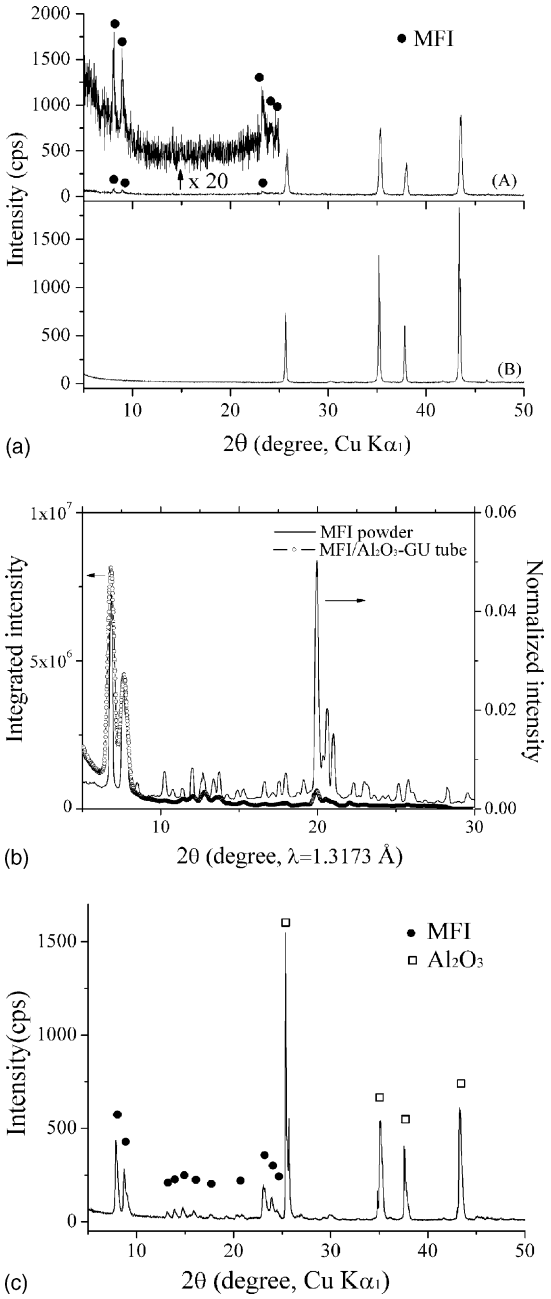

Fig. 3. PXRD patterns of cut pieces from the MFI/GU tube (A) and GU tube (B), using an in-house diffractometer (a), the PXRD pattern of the MFI/GU tube compared with the smoothed PXRD pattern of powder MFI, using the synchrotron X-ray source (b), PXRD pattern of a cut piece from the MFI/mesoporous-silica/CU tube, using an in-house diffractometer (c).

The morphology and thickness of the membranes were examined using scanning electron microscopy. For the MFI/meso-silica composite membrane, the SEM picture in Fig. 2b shows that the MFI layer deposited on the surface of a mesoporous-silica/CU tube is thinner than that on an MFI/GU tube. Further examining the Al_2O_3 layers of the support showed that a lot of small MFI crystals grew at interparticle pores and on particle surfaces of the Al_2O_3 macroparticles Fig. 2c and d). Fig. 3c shows a typical MFI pattern present with the Al_2O_3 support pattern on an MFI/meso-silica/Al_2O_3 tube through an in-house PXRD machine and a destructive method. This indicates that the small MFI crystals in the pores of the support can contribute strongly to in diffraction counts.

3.2. Nanostructured metal in mesoporous silica

The M41S materials exhibit one- and three-dimensional ordered channel systems, uniform apertures in the range of 2–10 nm, and surface area greater than 1000 m^2/g; and having thus expanded the pore-size-related applications of zeolites and zeolite-like molecular sieves to even bulkier reactants, the encapsulation of nanometer size guest compounds or clusters thus becomes possible.

Nanogold particles were prepared in one-dimensional mesoporous silica SBA-15 with pore diameter ~7 nm (as determined by N_2 adsorption and BJH method) and shown in Fig. 4, while nanostructured Pt metal was prepared in three-dimensional mesoporous MCM-48 of pore diameter ≅ 2.6 nm. Their synchrotron PXRD patterns (Figs. 5 and 6) indicate that Au and Pt metals possess the nanocrystalline nature.

With nano crystalline materials of size less than 10 nm, care must be taken for X-ray data collection and the Rietveld refinement, since the X-ray scattering power generated from nano size crystalline is weak and decays dramatically with

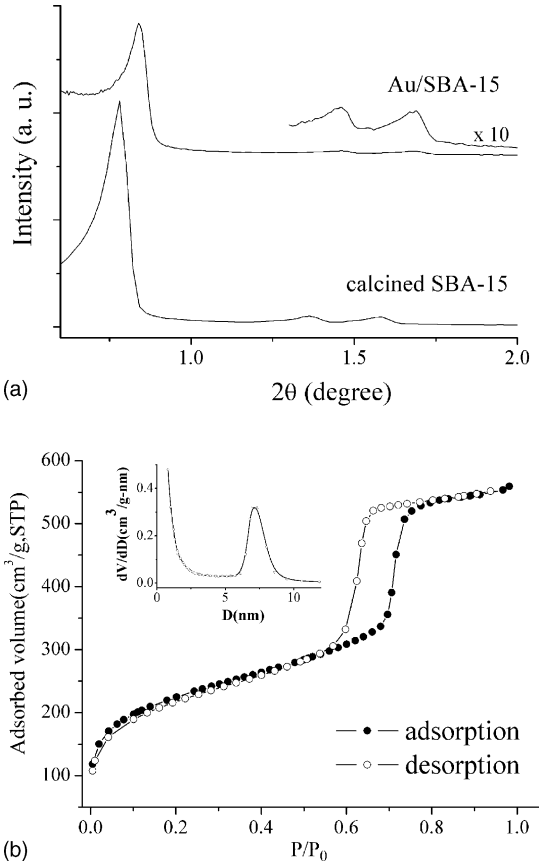

Fig. 4. Low angle PXRD patterns of SBA-15 and Au(8)-2/SBA-15 (a), and N_2 adsorption-desorption isotherm and pore size distribution (pore size distribution, dV/dD, vs. pore diameter, D) of SBA-15 (b).

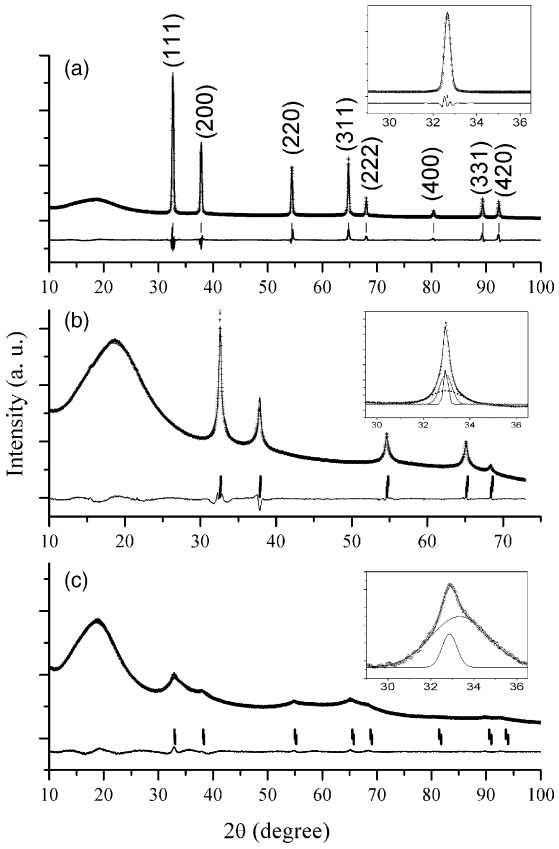

Fig. 5. Rietveld refinement of high angle synchrotron PXRD patterns and deconvolution of Au (1 1 1) peaks (inset) of Au nanoparticles in SBA-15 of Au2 (a), Au8-1 (b), and Au8-2 (c) samples.

size reduction in this range. To enhance the signal-to-noise ratio, a synchrotron X-ray source of high brightness is required. It is also better to collect diffraction data at wide angle using a linear detector or two-dimensional detector (used in this study). The intensity of the background signal can sometimes be higher than that generated from nano crystalline samples. Reducing the background contribution during data collection is thus quite important. Background can usually be derived from (1) amorphous impurities in samples, (2) the window of a capillary sample tube or polymer film, (3) air scattering, (4) instrument scattering such as from slits, etc [16]. A collimator with a very small aperture was placed in front of the sample and a beam stopper was placed very close to the sample in order to reduce the background contribution.

Fig. 5 shows the experimental PXRD data of nanostructured gold metals, the calculated patterns by the Rietveld refinement method and their differences in positions. Cell dimensions and particle sizes estimated from full widths at half maximum (FWHMs) of peak (1 1 1) reflection of Au in SBA-15 are listed in Table 1. Rietveld refinement converged to satisfatory values of R_p and wR_p. Particle sizes were calculated based on the FWHM of reflection peaks and

Table 1
Crystal parameters and particle sizes of Au nanoparticles in SBA-15.

Sample	Cell dimension (nm)	Rp	wRp	R_F2	Estimated size[a] (nm)	Peak area (%)
Au(2)	0.40804(1)	0.022	0.038	0.038	25 ± 1	100
Au(8)-1[b]	0.40807(1)	0.012	0.019	0.057	27 ± 2	17
	0.4073(1)				8 ± 2	37
	0.4067(5)				3 ± 2	45
Au(8)-2[b]	0.4074(1)	0.010	0.014	0.029	8 ± 2	15
	0.4062(1)				2 ± 1	85

[a] Based on FWHM of Au (1 1 1) reflection and Scherrer's equation $t = k\lambda/(B\cos\theta)$, where t = particle size, $k = 0.9$, B = FWHM in radians.
[b] The PXRD patterns of Au(8) samples were fitted into three or two profiles corresponding to different average sizes of Au metal.

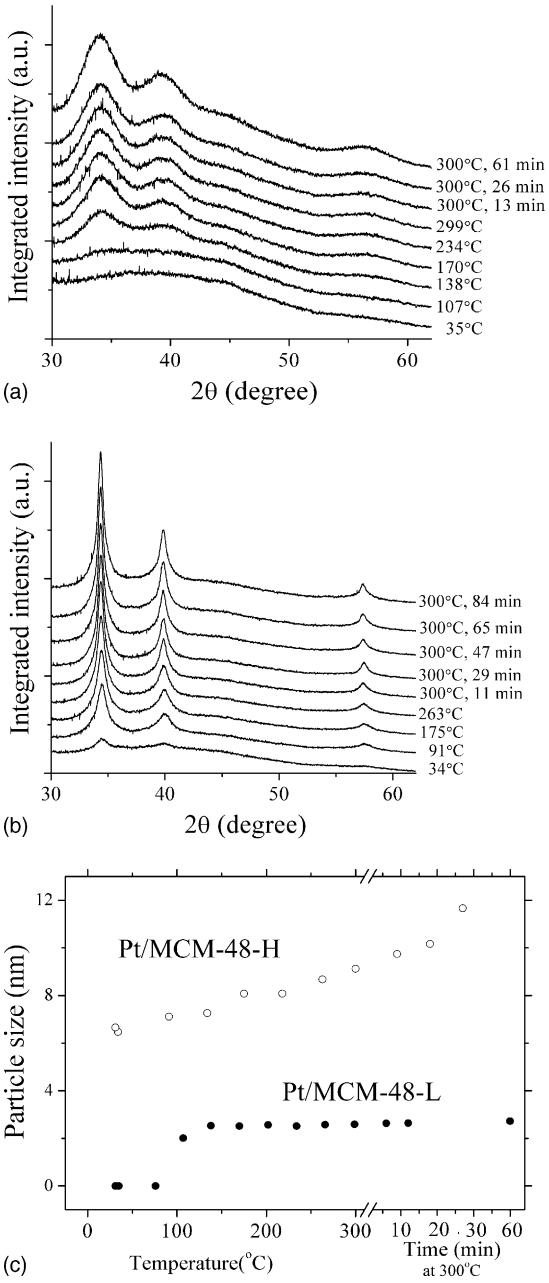

Fig. 6. In-situ PXRD study of the growth of nanostructured Pt in Pt/MCM-48-L (a) and Pt/MCM-48-H (b) samples. The temperature marks beside each profile were recorded at the beginning of each measurement. Some profiles were omitted due to no significant change compared with the previous one. The related variation of average Pt particle sizes vs. H_2 treatment temperatures on Pt/MCM-48 composites (c).

Scherrer's equation for the spherical model. The refined cell dimension of Au in the Au(2) composite is 0.40804(1) nm, a value close to 0.408 nm for the bulk metal, and larger than 0.4062 nm for Au in the Au(8)-2 composite. It has been suggested by Scardi and Antonucci [17] that as the crystal size of a metal becomes smaller, the compressive forces exerted by surface stress on it further reduce its lattice parameter, and this is in good agreement with the result of FWHMs. The smaller crystals have a large fraction of surface atoms, which draw the atoms tightly and reduce its unit cell dimension. Nanostructured Au and Pt were built based on the bulk fcc structure. PXRD shows the dimensions of Pt metal as 0.3927∼0.3931 nm in Pt/MCM-48 composites. The bond distances of Au–Au and Pt–Pt pairs are 2.87 and 2.77 Å, respectively. Thus, the cell dimension of nanosized Au particles is larger than that of nanostructured Pt.

The Rietveld refinement on Au(2) used a single phase, while Au(8)-1 & Au(8)-2 were refined by employing three and two sizes of nanoparticles and were found to consist of 3 ± 2 nm (major componet), 8 ± 2 nm (major component), & 27 ± 2 nm and 2 ± 1 nm (major component) & 8 ± 2 nm metal particles for Au(8)-1 and Au(8)-2, respectively as shown in Fig. 5 and Table 1. These results are in good agreement with TEM images as shown in Fig. 7. On the contrary, the Au particles in Au(2) have an average size of 25.5 nm, much larger than the aperture of SBA-15 (7 nm), and may thus exist at the external surface of SBA-15 as shown in Fig. 7.

3.3. In-situ PXRD of Pt nano-particle growth in MCM-48

The crystal growth of Pt metal in three dimensional mesoporous MCM-48 was further monitored by an in-situ PXRD. In Fig. 6 the high angle PXRD profiles of Pt/MCM-48-L measured at a temperature range of 35–300 °C are shown. The earliest appearance of distinguishable metal peaks can be found in 107–138 °C profiles. It means that Pt precursor can be reduced in this temperature range. The FWHM of the Pt (1 1 1) diffraction peak in each profile can be further analyzed by Scherrer's formula to estimate the average particle size of Pt metal. The relations between estimated particle sizes and in-situ reduction temperatures are shown in Fig. 6c. The particle size estimated from the 138∼170 °C profiles is ∼2.5 nm and did not change much in the temperature range from 138 to 300 °C, but the intensity of the Pt(1 1 1) peak and the number of ∼2.5 nm particles increased with the heating time at 300 °C. In the Pt/MCM-48-H sample, the reduction at room temperature under pure hydrogen flow produces broad and weak diffraction peaks as shown in the lower temperature profiles. The sizes of Pt metal particles have been found to increase from 6 nm to 9 nm (estimated from Pt (1 1 1) peaks) upon increasing the temperature from 35 to 300 °C, furthermore, the size of particles increased with heating time at 300 °C. It is suggested that for low Pt loading of Pt/MCM-48-L, small nano-particles of Pt metal do not easily aggregate and form large particles. With higher Pt loading in Pt/MCM-48-H Pt can aggregate into metal nanobars or nanonetworks inside the channels of MCM-48 during higher temperature treatment. The concentration of H_2PtCl_6 precursor for Pt/MCM-48-H is 2.0 M rather than 0.1 M for Pt/MCM-48-L, and this, in turn, may induce defect sites in the host by the damage of MCM-48 through high acidity (pH = 1). The migration and aggregation of nanosized Pt metal might be enhanced at the defect sites of the host.

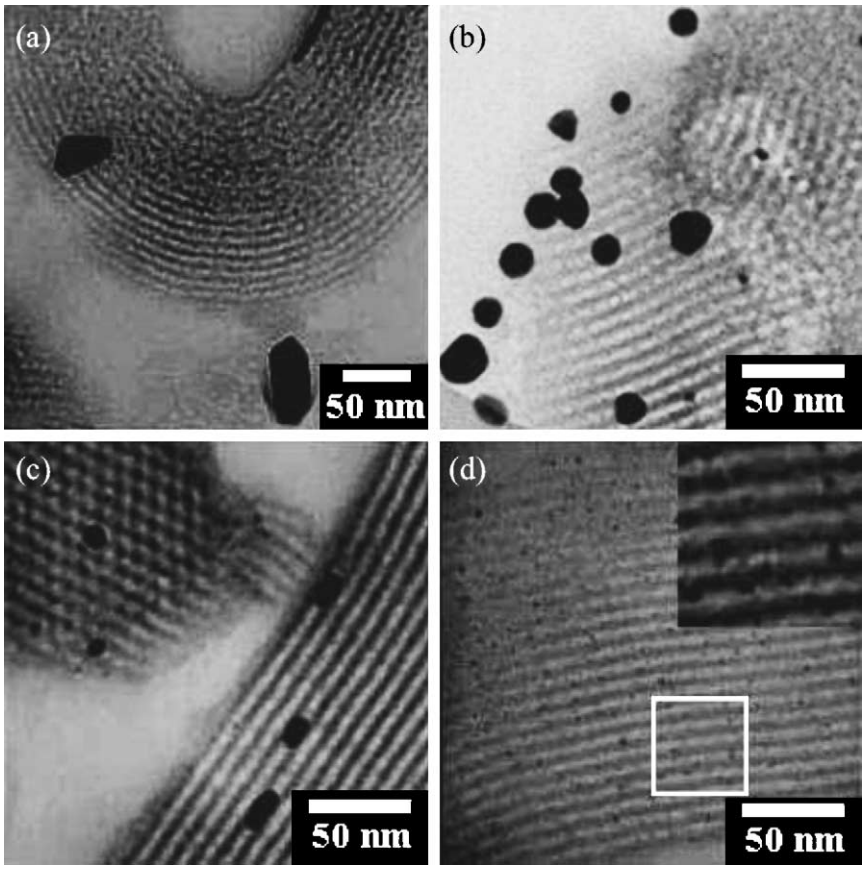

Fig. 7. TEM images of Au(2) along the [1 1 0] zone axes of SBA-15 (a), Au(8)-1 along the [1 1 0] zone axes (b), Au(8)-2 along the [1 0 0] and [1 1 0] zone axes (c), and Au(8)-2 along the [1 1 0] zone axes (d).

4. Conclusion

In summary, a synchrotron X-ray source has been demonstrated to be useful in the characterization of very thin films of zeolite crystals and small amounts of nanostructured metal. Moreover, the cell dimension of the nanostructured metal has been found to vary with its size, and the relative intensity of crystalline MFI to Al_2O_3 support is dependent on its location in tubular samples.

References

[1] G. Margaritondo, "Elements of Synchrotron Light for Biology, Chemistry and Medical Research" (2002), Oxford University Press.
[2] P. Norby, J.C. Hanson, Catal. Today 39 (1998) 301.
[3] J.R. Helliwell, Acta Cryst. A54 (1998) 738.
[4] H. Marjorie, Acta Cryst. B51 (1995) 432.
[5] D. Loue, Acta Cryst. A54 (1998) 922.
[6] H.M. Rietveld, J. Appl. Crystallogr. 2 (1969) 65.
[7] C.M. Yang, H.S. Sheu, K.J. Chao, Adv. Funct. Mater. 12 (2002) 143.
[8] D.Y. Zhao, J.L. Feng, Q.S. Huo, N. Melosh, G.H. Fredickson, B.F. Chmelka, G.D. Stucky, Science 279 (1998) 548.
[9] C.M. Yang, P.H. Liu, Y.F. Ho, C.Y. Chiu, K.J. Chao, Chem. Mater. 15 (2003) 275.
[10] R. Ryoo, S.H. Kim, J. Phys. Chem. B. 103 (1999) 7435.
[11] A.C. Larson, R.B. von Dreele, "Generalized Structure Analysis System," (1994), Los Alamos National Laboratory, Los Alamos, NM.
[12] S.T. Sie, Stud. Surf. Sci. Catal. 85 (1994) 587.
[13] G. Ertl, H. Knözinger, J. Weitkamp (Eds.), Handbook of Heterogeneous Catalysis, vol. 1, VCH Co., Weinheim, 1997, pp. 286–386.
[14] A.S.T. Chiang, K.J. Chao, J. Phys. Chem. Solids 62 (2001) 1899.
[15] D. Casnave, A. Giroirfendler, J. Sanchez, R. Loutaty, J.A. Dalmon, Catal. Today 25 (1995) 309403.
[16] L.B. McCusker, R.B. Von Dreele, D.E. Cox, D. Louer, P. Scardi, J. Appl. Crystallogr. 32 (1999) 36.
[17] P. Scardi, P.L. Antonucci, J. Mater. Res. 8 (1993) 1829.